Plasmonic Chemically Modified Cotton Nanocomposite Fibers for Efficient Solar Water Desalination and Wastewater Treatment

Nanoscale

Plasmonic Chemically Modified Cotton Nanocomposite Fibers for Efficient Solar Water Desalination and Wastewater Treatment

Hiran D Kiriarachchi[a], Fathi S. Awad[a,b], Amr A Hassan[a,c], Julian Bobb[a], Andrew Lin[a], and M. Samy El-Shall*[a]

Water desalination and wastewater treatment via solar photothermal energy conversion are among the most important technologies to address the increasing pressing global water scarcity. Solar energy is the cleanest, most abundant, renewable natural resource available. Herein, we report the development of highly efficient, flexible, low weight, and cost effective *Plasmonic Functionalized Cotton (PFC)* nanocomposite materials for solar steam generation through the efficient evaporation of surface water pools. The PFC nanocomposites contain metallic nanoparticles that exhibit strong solar absorption followed by non-radiative relaxation causing the absorbed energy to be converted into heat for efficient water evaporation. The chemically modified cotton leads to a partial hydrophobic surface that allows the material to float on the water's surface and provide excellent thermal insulation properties in addition to facile and scalable synthesis. The PFC nanocomposites containing Au and Ag nanoparticles are demonstrated to be among the most efficient solar thermal converters reported to date for solar water desalination. The Au/Ag-PFC fibers exhibit average water evaporation rates of 1.4 and 11.3 kg m^{-2} h^{-1} with superb solar thermal efficiencies of up to 86.3% and 94.3% under 1 and 8 sun illumination, respectively. Furthermore, the Au/Ag-PFC fibers display stable evaporation rates over more than 10 repeated evaporation cycles without any performance decline under acidic solution at pH 2 or basic solution at pH 10. The successful application of the Au/Ag-PFC fibers for the removal of organic dyes from contaminated water through the solar steam generation is also demonstrated. The high solar thermal evaporation efficiency, excellent stability and long-time durability make the PFC nanocomposites excellent candidates for applications in seawater desalination and wastewater treatment by solar-steam generation.

Solar steam generation and solar desalination are among the most important technologies to address the increasing pressing global water scarcity.[1-3] Solar energy is the cleanest, most abundant, renewable natural resource available. The basic principles of solar water desalination are based on the way nature makes rain.[3] The sun's energy heats water to the point of evaporation and as the water evaporates, water vapor rises where it condenses on a glass surface for collection. Materials for solar photothermal energy conversion are highly sought after for their broad utility in providing water heating and/or steam for many applications including domestic water heating and wastewater treatment.[1-3] Additional uses include solar-driven desalination and solar steam for industrial purposes, solar crop drying technologies, and basic solar stills to purify water in remote regions.[1-3]

Extensive research has been focused on the development of broad solar absorption materials with flexible, porous, and low weight properties that can float on the water's surface to provide more efficient and cost effective solar thermal systems.[4-8] Metal nanoparticles have been proposed to take advantage of the high efficiency of the photothermal energy conversion associated with Surface Plasmon Resonance (SPR) absorption.[9-14] Several examples of noble-metal and carbon-based nanofluids have been demonstrated for solar steam generation.[15-18] Nanostructured carbon-based materials such as carbon nanotubes, graphene oxide (GO) and reduced GO (RGO) have recently been applied in photothermal energy conversion as they can absorb light over the visible and near infrared (NIR) parts of the electromagnetic spectrum and convert the absorbed radiation into heat through nonradiative decay processes with excellent photothermal transduction properties.[5,19-23] Plasmonic-graphene nanocomposite films have been demonstrated to be effective for the efficient conversion of solar energy into usable heat for water evaporation and steam generation.[24] The drawback of these materials is the complicated synthesis methods and associated high cost of the resulting materials. On the other hand, cellulose from cotton biomass waste can be a cost effective host material for plasmonic nanoparticles. However, cotton fibers are highly hydrophilic because of the oxygen-containing cellulosic functional groups on the surface of the fibers.[25,26] Thus cotton takes up water very rapidly and tends to sink in water.[25] Herein, we report the successful development of a new highly efficient, flexible, low weight and cost effective Plasmonic Functionalized Cotton (PFC) nanocomposite fibers for solar water desalination and for wastewater treatment. In this work, we introduce partially hydrophobic cotton as a host material for metal nanoparticles to generate the PFC nanocomposite fibers as novel photothermal materials. The developed PFC fibers float on the surface of seawater and, at the same time, allow water to be transported by capillary forces through the fibers to the external surface for solar thermal evaporation. Here, we demonstrate that these materials can significantly enhance the absorption of the solar

a. Department of Chemistry, Virginia Commonwealth University, Richmond, Virginia 23284, United States.
b. Chemistry Department, Faculty of Science, Mansoura University, Mansoura 35516, Egypt
c. Chemistry Department, Faculty of Science, Ain Shams University, Cairo 11566, Egypt

energy and the high conversion efficiency of sunlight into heat. These materials also offer advantages over the less durable polymeric materials which have the limitation of high temperatures and challenges of the long-term stability and weathering during operation.

Materials and Methods

Materials. Commercial cotton, 2,4-toluene diisocyanate (TDI, 95.0%), anhydrous dimethylformamide (DMF, 99.8%), gold (III) chloride solution (99.99%), silver nitrate (99.0%), hydrazine hydrate (80%), magnesium sulfate (99.99%), calcium chloride (99.9%), sodium chloride (>99.0%). All reagents were purchased from Sigma-Aldrich and used without further purification. Deionized (DI) water was used in all the experiments.

Synthesis of TDI-Cotton. In a typical synthesis, commercial cotton fibers were cut into squares (5×5×1 cm) and washed with anhydrous DMF to remove impurities and traces of water. Then the cotton squares were immersed in 25 mL of anhydrous DMF containing excess TDI for 24 hours. Modified cotton samples then washed with DMF and dried under ambient conditions.

Synthesis of Plasmonic TDI-Cotton. To synthesize 5% Au-TDI-Cotton or 5% Ag-TDI-Cotton samples, a TDI-cotton sample was first weighed and then immersed in a 25 mL solution containing appropriate amounts of gold chloride or silver nitrate for 6 hours. Then the samples were mildly washed with deionized water and re-immersed in 25 mL of fresh DI water. To reduce the metal ions, 25 μL of hydrazine hydrate was added and the solution was microwaved using a 700 W microwave oven for 60 s (in 10 s intervals). Afterwards, the samples were washed several times with cold water then dried overnight at room temperature.

Characterization. The TDI-Cotton fibers were characterized using the FT-IR spectroscopy using the Nicolet-Nexus 670 FTIR spectrometer (4 cm^{-1} resolution and 32 scans) diamond attenuated total reflectance (DATR). The morphology of the cotton fibers with and without plasmonic nanoparticles was characterized by SEM (Hitachi SU-70 FE-SEM). The optical characterization of the plasmonic cotton fibers was determined using a superior micro spectrophotometer (Olis 14 CD), with reflectance power supply (CRAIC Technology, 75 W Xenon). A Newport Sol2A solar simulator with a power of 450 W was used as the source of natural sunlight for all the steam generation experiments. The concentration of metal ions in solution before and after desalination was determined by inductively coupled plasma-optical emission spectrometry (ICP-OES).

Solar Steam Generation Experiments. The experimental set up using the solar simulator 450 W, Newport Sol2A, Class ABA is shown in

Figure S1 (Supporting Information). The solar steam generation rates of three solar absorber cotton samples Au-f-C, Ag-f-C and Ag/Au-f-C were measured and compared with pure deionized water under three solar irradiation intensities of 1, 5 and 8 kW/m^2 over 30 min. The different solar intensities were obtained using a focusing lens (208.2 mm focal length and 279.4 mm diameter). The sample with a diameter of 6 cm and thickness 1.5 cm was floated on top of the water surface in a 50 mL petri dish filled with pure deionized water placed on a calibrated electronic balance. The temperatures of the steam (evaporation surface) and bulk water (water below the sample) were recorded using an IR heat sensor and a thermocouple, respectively. The evaporation rate was calculated as the change in the recorded mass of water normalized by area of the irradiated sample and the corresponding time interval. The weight changes were determined (recorded) at the corresponding time interval (5 min) and then used to calculate the evaporation rate and efficiencies of the solar vapor generation. All the experiments were carried out at room temperature of 20 ± 1 °C and humidity of ~40%.

Solar Water Desalination Experiments (SWD). To evaluate the potential of the plasmonic cotton in seawater desalination, a sample of modelled seawater containing 1500 ppm Mg^{2+}, 1250 ppm Ca^{2+}, and 1000 ppm Na$^+$ was used for the steam generation experiment. A glass chamber with an angled hood was utilized to condense the generated steam which was later collected by a clean pipette. Condensed steam sample was carefully analysed by inductively coupled plasma optical emission spectroscopy (ICP-OES) to determine the concentration of the primary ions (Na$^+$, Mg^{2+}, and Ca^{2+}) naturally existing in the seawater.

Waste Water Treatment. To evaluate the application in waste water treatment, plasmonic cotton samples were tested in two experiments. In the first experiment, steam generation was carried out using water at extreme pH values of 2 and 10 using acidic and basic solutions of HCl and NaOH, respectively. In the second experiment, a dye solution (methylene blue, 10 ppm) was used as a model of a polluted water sample. Steam generation experiment was carried out using the dye solution instead of deionized water at 5 kW m^{-2} solar intensity and the absorption spectra of the dye solution and the steam were compared to evaluate the purification.

Solar Steam Generation Recycling Experiments. Ten solar steam generation cycles were carried out to evaluate the sustainability and stability of the Ag/Au-f-C sample. In each cycle, the cotton sample was illuminated under solar light supplied by the solar simulator (Sol2A, Newport) with a light density of 5 kWm^{-2} for 30 minutes and the weight changes of water and the temperature of the steam were determined. After each cycle the sample was cooled down under ambient conditions for the next cycle.

ARTICLE
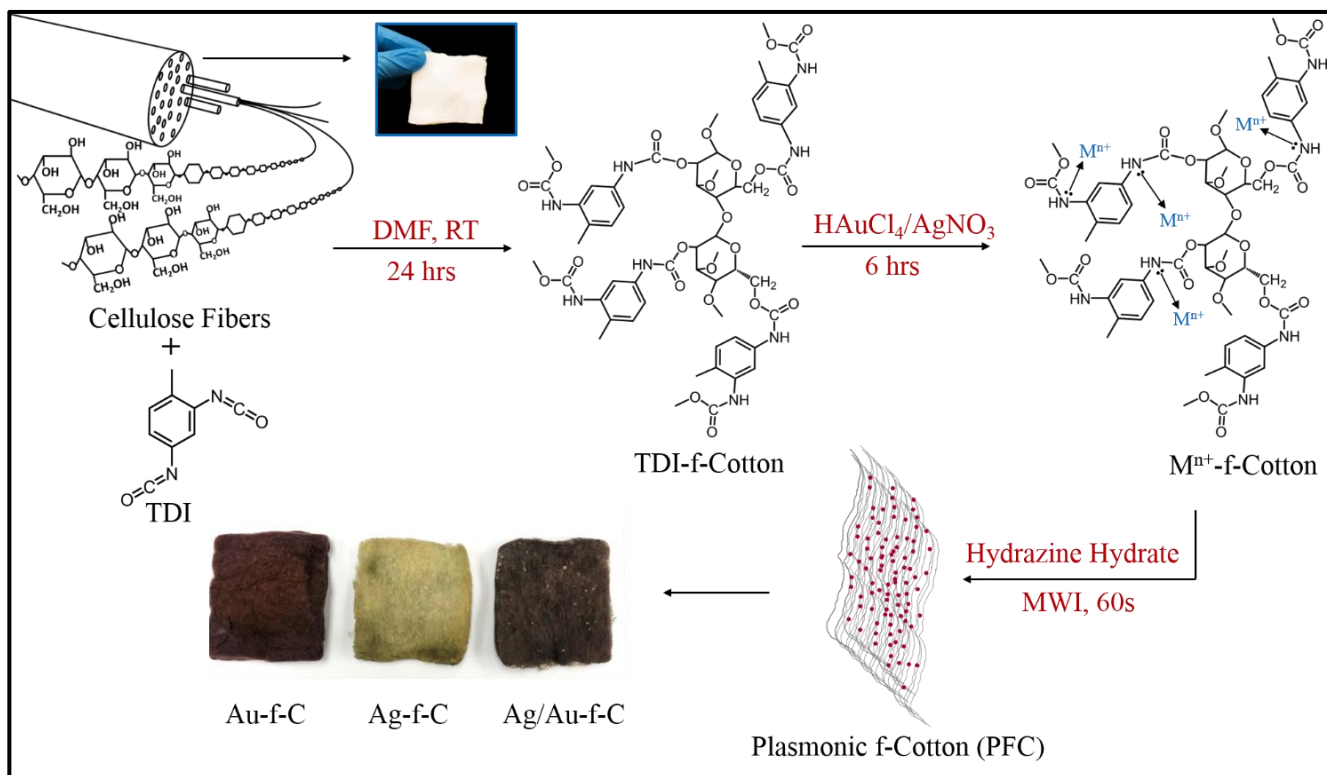
Figure 1. Design strategy and general steps involved in the synthesis of PFC samples.

Results and Discussion

A schematic representation for the general synthesis of the plasmonic functionalized cotton (PFC) fibers is described in Figure 1. The design strategy involves the covalent attachment of the isocyanate groups of the 2,4-toluene diisocyanate (TDI) molecules to the cellulose fibers through the formation of a stable urethane linkage between TDI and the hydroxyl groups emerging from the cellulose fibers. The TDI molecules contain phenyl hydrophobic groups which replace some of the hydrophilic groups present on the surface of the cotton fibers. Therefore, the TDI functionalization of the cotton fibers changes the character of the fibers from intrinsically hydrophilic to partially hydrophobic which can then float on the surface of water allowing spontaneous flow of water through the fibers driven by a capillary force. To provide a strong solar absorber to enable efficient photothermal energy conversion, plasmonic Au and Ag nanoparticles are anchored to the surface of the TDI-modified cotton fibers through strong electrostatic adsorption of the Au and Ag ions by the amino and amide functional groups of the functionalized cotton fibers. The next step involves the rapid reduction of the metal ions on the surface of the TDI-modified cotton fibers by hydrazine hydrate under fast microwave heating (50 s). The rapid reduction of the adsorbed metal ions is expected to lead to pulsed nucleation under limited growth conditions due to the low concentration of the metal ions thus resulting in the formation of well-dispersed plasmonic nanoparticles within the PFC fiber.[27]

The successful modification of the cotton fibers to become partially hydrophobic is illustrated in Figure 2 which shows the difference of buoyancy of pure cotton and TDI functionalized cotton fibers (A video is included in the supplementary materials). It is clear that the TDI-functionalized

cotton takes up much less water than the un-functionalized pure cotton. The process of water transport in the un-modified pure cotton is described by a sequence of capillary-driven convection over the external surface, radial flow between the fibers along the length, and diffusion into the individual fibers leading to extensive uptake of water which results in sinking of the wet cotton in water.

**Figure 2.** Difference of the hydrophilicity of the pure cotton and TDI functionalized cotton.

The FT-IR spectra of pure cotton and TDI functionalized cotton fibers are shown in Figure 3. The broad peak from 3100-3500 cm^{-1} and the strong shoulder peak around 1050 cm^{-1} are attributed to the O-H and C-O stretching vibrations of hydroxyl functional groups of cellulose fibers, respectively. The TDI functionalized cotton fiber also shows a less prominent peak in the same range as of the O-H stretching vibrations indicating

that the material still has some hydroxyl groups left to maintain hydrophilicity to channel water to the evaporation surface. The introduction of the urethane linkage between cotton fibers and TDI molecules is evident by the peaks around 1710 and 1535 cm^{-1} which are attributed to the C=O stretching vibrations and N-H bending respectively as shown in the magnified spectrum presented in Figure 3B.[28,29] Therefore, the presence of the C=O and N-H bending peaks proves the successful functionalization of the cotton fibers.
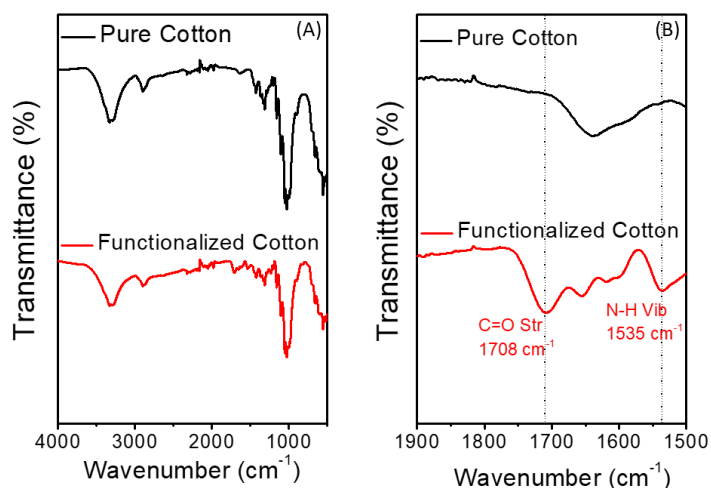

Figure 3. FT-IR spectra of pure cotton and TDI functionalized cotton. (A) Full scale, (B) Expanded region between 1500 cm^{-1} and 1900 cm^{-1}

Figures 4(A) and 4(B) display the UV-vis absorption spectra of the Au-f-C and Ag-f-C nanocomposite fibers. Both the Au-f-C and Ag-f-C fibers exhibit considerably broad absorption bands with peak maxima around 538 and 437 nm corresponding to the SPR bands of Au and Ag nanoparticles, respectively.[30,31] The absence of a capping agent during the synthesis of the nanoparticles results in wide size distributions and broad SPR absorption bands. However, broad SPR absorption bands can be beneficial for applications that harness solar energy since the material can utilize a significant portion of the solar spectrum and effectively convert the photon energy into thermal energy, thus the solar to steam conversion efficiency can be significantly increased. Moreover, having both gold and silver nanoparticles in the same composite fiber can effectively increase the utilized range of the solar spectrum.[24] Figure 4(C) displays the reference solar radiance spectrum (under AM 1.5 G)[32] with the UV-visible absorbance spectra of the Au-f-C and Ag-f-C fibers shown in the inset. It is clear that the maximum absorbance of the Au-f-C and Ag-f-C samples lies in the spectral region with the highest solar irradiance which is beneficial for the effective photo-thermal energy conversion.
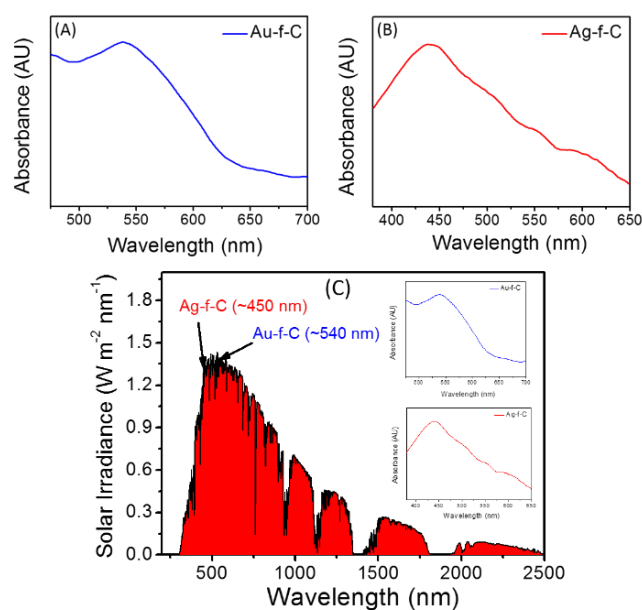

Figure 4. UV-Vis absorption spectra of (A) Au-f-C, (B) Ag-f-C nanocomposite fibers and (C) Solar spectral irradiance (AM 1.5 G) with the UV-Vis absorption spectra of the Au-f-C and Ag-f-C fibers (inset).

The surface compositions of the Au-f-C and Ag-f-C nanocomposites are further analyzed using X-ray photoelectron spectroscopy (XPS). The Au 4f spectrum displayed in Figure 5(A) clearly shows the presence of Au^0 nanoparticles within the Au-f-C composite. The strong doublet at 84.5 eV and 88.1 eV corresponds to the Au 4f$_{7/2}$ and Au 4f$_{7/2}$ states of Au^0. The less prominent doublet (89.5/86.2 eV) is ascribed to the surface oxidized Au^{3+} ions. The broadness of the Au^{3+} peaks relative to those of Au^0 could be explained by the chelation of Au^{3+} ions by the amine groups present in the functionalized cotton.[33,34] The Ag 3d spectrum of the Ag nanoparticles, displayed in Figure 5(B), consists of two main peaks at 368.1 eV and 374.1 eV which are assigned to the Ag 3d$_{5/2}$ and 3d$_{3/2}$ states, respectively.[35] The two small peaks at 375.5 eV and 370.2 eV are most likely due to the presence of a small fraction of silver oxide species. Since the samples are stored under ambient conditions, the formation of an oxide layer over the surface of the Ag nanoparticles is inevitable.[36] However, it is also possible that these peaks represent the strong association of silver ions with the amine groups of the urethane bond.[37]
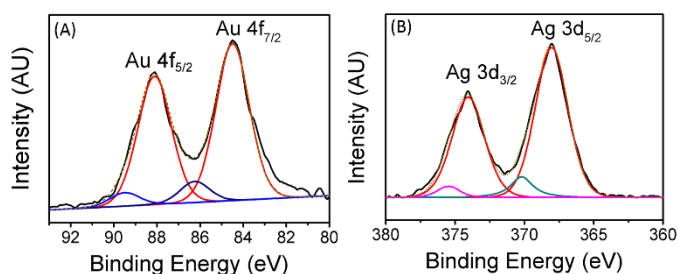
Figure 5. XPS spectra of the Au 4f electron (A) and the Ag 3d electron (B) in the Au-f-C and Ag-f-C fibers, respectively.
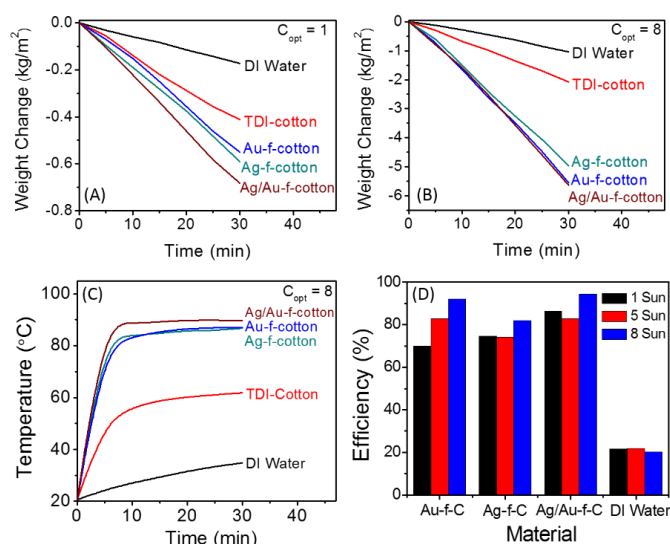
SEM images of the TDI-functionalized cotton fibers and the Au-f-C and Ag-f-C nanocomposite fibers are shown in Figure 6. According to the SEM images, the size distributions of the Au and Ag nanoparticles are in the range of 70 to 100 nm with no evidence of agglomeration. Also, it is evident that the nanoparticles are uniformly distributed on the surface of the functionalized cotton fibers. Compared to support materials with a planar morphology, materials with fibrous morphology provide a higher surface area support for the dispersion of the nanoparticles.[24] Also, the introduction of the amine and amide functionality to the cotton fibers facilitates the chelation of the plasmonic metal ions on the surface of the cotton fibers uniformly.
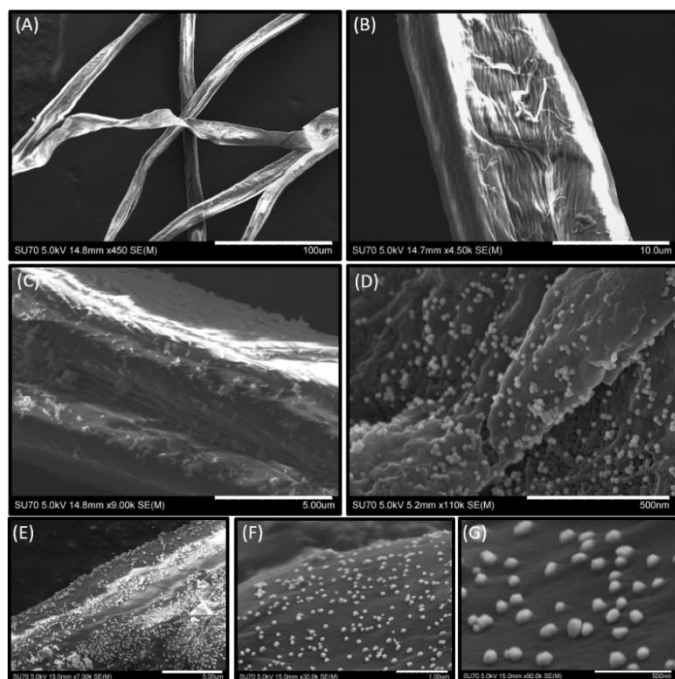
Figure 6. SEM images of nanoparticle free functionalized cotton fibers (A and B), Au-f-C nanocomposites (C and D) and Ag-f-C nanocomposites (E-G). The scale bars of the images A to G are 100, 10, 5, 0.5, 5, 1 and 0.5 μm, respectively.

To evaluate the solar steam generation efficiency for different PFC solar thermal converters, four samples of nanoparticle-free functionalized cotton (f-cotton), Au-functionalized cotton (Au-f-C), Ag-functionalized cotton (Ag-f-C), and Ag/Au-functionalized cotton (Ag/Au-f-C) nanocomposites were tested. All the samples were tested for steam generation and compared with pure deionized water in the absence of any solar absorber under three different solar illuminations of 1 kW/m^2 (1 sun), 5 kW/m^2 (5 sun) and 8 kW/m^2 (8 sun) over 30 min using the solar simulator 450 W, Newport Sol2A, Class ABA. Figure S2 (Supporting Information) displays digital images for the steam generation by the PFC samples, and a video showing steam generation from the water surface using the Ag/Au-f-C fiber is provided in the Supporting Information. The results presented in Figures 7(A) and 7(B) display the normalized steam generation rates at solar illumination of 1 kW m^{-2} (1 sun) and 8 kW m^{-2} (8 sun), respectively (the results obtained at 5 sun are shown in Figure S3 (Supporting Information). At all solar illumination intensities, the pure cotton exhibits the lowest evaporation rate (0.82 and 4.16 kgm$^-$

^{2} h^{-1} at 1 and 8 sun, respectively) due to the lack of solar absorption by the cotton. The small enhancement effect in the evaporation rate over pure water (2 times at 1 sun) is attributed to surface evaporation through the porous structure of the fibers which results in minimizing the heat loss by bulk water. Anchoring plasmonic nanoparticles on the functionalized cotton surface significantly enhances the rates of solar steam generation compared to the control sample. At one sun, the Ag/Au-f-C sample could evaporate water at a rate of 1.4 kg m^{-2} h^{-1} whereas plasmonic free functionalized cotton could only evaporate about 0.8 kg m^{-2} h^{-1}. At 8 sun, the difference is even higher showing an evaporation rate 2.8 times higher than the plasmonic free sample. Under all the solar intensities, Ag/Au-f-C sample demonstrated the highest steam generation rates (1.4, 6.7 and 11.3 kg m^{-2} h^{-1} under 1, 5 and 8 sun, respectively). The enhanced efficiency of the Ag/Au-f-C sample is due to the presence of both Au and Ag nanoparticles as plasmonic absorbers within the cotton nanocomposite fibers. As shown in Figure 4, Au and Ag nanoparticles possess different absorption maxima in the visible spectra. Therefore, Ag/Au-f-C fibers which contain 1:1 mixture of Au and Ag nanoparticles can harness a much larger portion of the solar spectrum compared to the PFC samples containing only one type of plasmonic nanoparticles. The low thermal conductivity of the cotton fibers (0.065 W/mK) also helps the PFC samples to isolate the heat and minimize the heat loss to bulk water.[37]

Figure 7. Solar steam generation data for different PFC samples under different solar intensities (A) 1 kW m^{-2} (optical concentration C_{opt} = 1), and (B) 8 kW m^{-2} (optical concentration C_{opt} = 8). (C) Temperature change at the surface of different PFC samples and DI water after solar illumination for 30 min under optical concentrations of C_{opt} = 8. (D) The evaporation efficiency of different PFC samples under 1, 5, and 8 kW m^{-2} solar illumination.

Figure 7(C) displays the temperature profiles of the different samples on the irradiation surface at the solar intensity of 8 kW m^{-2}. The results for the surface temperatures of the samples at the solar intensity of 1 kW m^{-2} are shown in **Figure S4** (Supporting Information). The trend observed in the surface temperature profile correlates with the general trends of the steam generation rates shown in Figures 7(A) and 7(B). The Ag/Au-f-C sample exhibits the highest surface temperature rise at 8 sun illumination. After 5 minutes of irradiation, the surface temperature of the Ag/Au-f-C

sample increases from 20.6 to 88.8 °C while the blank water sample only changes from 20.5 to 24.4 °C after the same period of illumination time. Under 1 sun intensity, the maximum surface temperatures of the Au-f-C, Ag/Au-f-C, Ag-f-C samples after 30 min of illumination time reach 31.8, 30.5 and 30.0 °C, respectively. These low temperatures indicate the high evaporation efficiency of the PFC fibers under 1 sun.

Figure 7(D) compares the solar-to-vapor efficiencies of the PFC fibers at three solar intensities (1, 5 and 8 sun). The thermal efficiency η_{TH} is defined as (η_{TH} = m h_{LV} / C_{opt} q_i) where m represents the mass flux in g m^{-2} s^{-1}, h_{LV} is the total enthalpy for the liquid to vapor phase change of water in J. C_{opt} is the optical concentration (number of suns) and q_i the nominal direct solar intensity (generally considered as 1 sun = 1 kW m^{-2}).[18-20] The results reveal that the Ag/Au-f-C sample exhibits the highest thermal efficiencies of 86.3, 82.9 and 94.3 % for solar enabled steam generation under 1, 5 and 8 sun, respectively. The calculated efficiency at 8 sun is considered one of the highest values reported for photothermal energy conversion materials used for solar water desalination.[12,18-24,38,39]

Under solar intensity of one sun, the Ag/Au-f-C sample exhibits a solar-to-vapor efficiency of 86.3% with only about 14% loss of energy due to reflection of the incident light, conduction and convection.[8] Reflection measurements of the Ag/Au-f-C sample indicated an average percentage reflection around 20% in the spectral regions where they exhibit the maximum absorbance. As shown in the **Figure S4**, the maximum surface temperature of the Ag/Au-f-C sample after 30 min irradiation is measured as 30.5 °C while the average bulk temperature of water is 22.2 °C. Using the average length of the conductive path of the PFC samples as 1 cm and assuming the PFC sample possess a similar thermal conductivity as of pure cotton (0.026 W/m K),[37] the conductive heat flux for the Ag/Au-f-C sample can be calculated as 21.6 W m^{-2}. Considering the input solar intensity at 1 sun (1 kW m^{-2}), the calculated conductive heat loss is only ~ 2.2%. Temperature difference between the bulk water and the irradiation surface is a critical factor for the magnitude of heat loss by convection and irradiation. However, since after 30 minutes of irradiation under 1 sun the temperature difference between the sample surface and bulk water is found to be only ~8 °C, the convection and radiation heat loss can be estimated as 8% comparable to carbonized mushrooms materials.[8]

To further evaluate the utility of the PFC fibers in solar seawater desalination and wastewater treatment, the concentrations of the three primary ions Na$^+$, Ca^{2+} and Mg^{2+} naturally present in seawater were determined in the condensed water obtained from the desalination system using inductively coupled plasma-atomic emission spectroscopy (ICP-OES). Figure 8(A) shows that the concentrations of the representative ions are significantly reduced after the solar water desalination (SWD) using the Ag/Au-f-C fiber. The concentrations of the Na$^+$, Ca^{2+} and Mg^{2+} ions decreased significantly from the original values of 1000, 1250 and 1500 mg/L to 0.05, 0 and 0.1 mg/L, respectively after the SWD. The ion concentration values after the SWD by the PFC are well below the standard values reported by the US Environmental Protection

Agency (EPA) and the World Health Organization (WHO), as well as below the values obtained by common seawater desalination techniques such as membrane (10–500 ppm) and distillation (1–50 ppm).[5,12,40] Figure 8(B) represents the reusability test done for the Ag/Au-f-C sample in seawater desalination. According to the results, the Ag/Au-f-C sample retains its stability over ten desalination cycles without any performance change. This excellent stability and reusability demonstrate that the PFC fibers are highly suitable for various applications in solar seawater desalination and steam generation.
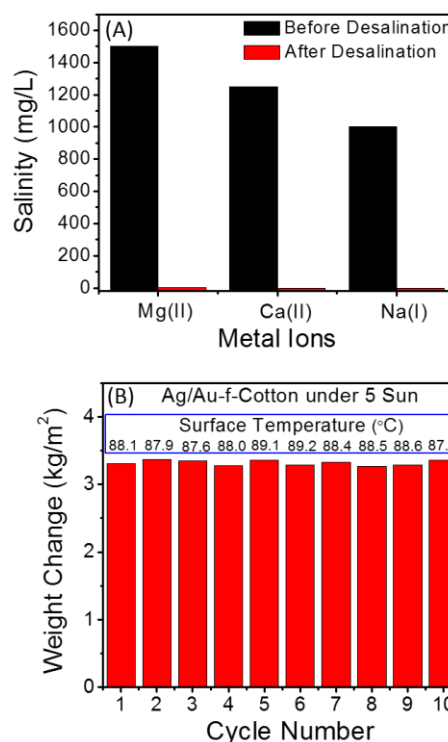
Figure 8. (A) Concentration of three primary metal ions in an artificial sea water sample before and after desalination and (B) Recyclability test of the Ag/Au-f-C sample during 10 cycles under constant illumination of 5 kW m^{-2} for 30 minutes.

Finally, the utility of the Ag/Au-f-C sample was also tested for SWD under acidic and basic environments and for the purification of wastewater containing an industrial dye. As shown in Figure 9(A), the Ag/Au-f-C sample could function in an acidic solution at pH 2 or in a basic solution at pH 10 under a solar intensity of 5 kW m^{-2} for 30 minutes without any significant performance deterioration. Steam generation rates at pH 2, 7 and 10 were 6.72, 6.70 and 6.84 kg m^{-2} h^{-1}, respectively. Gold and Silver metal nanoparticles are well known for their inherent resistance to acidic and basic environments.[41,42] Therefore, the PFC fibers can be ideal candidates for solar driven steam generation techniques that can be used for wastewater treatment. Figure 9(B) demonstrates the successful application of the Ag/Au-f-C sample in the solar purification of contaminated water containing the model pollutant methylene blue dye. The absorption spectra of the polluted water containing 10 ppm methylene blue dye and the condensed steam sample after the solar illumination clearly confirms the complete removal of the dye from the condensed steam sample.
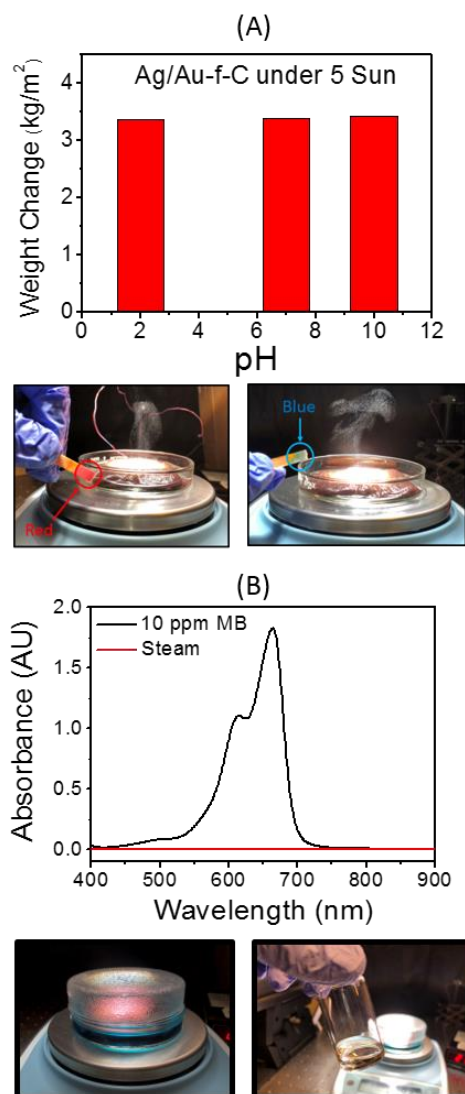
Figure 9. Applications of the PFC materials (Ag/Au-f-C as the representative sample) in waste water treatment. (A) Stability of the Ag/Au-f-C sample in extreme pH values (pH 2 and 10) and (B) UV-vis spectra of the model pollutant methylene blue, before the steam generation experiment and after condensation of the steam.

Conclusions

In conclusion, we designed and developed a new class of PFC nanocomposite fibers for the efficient solar water desalination. With the characteristics of high optical absorption, low thermal conductivity, effective water transmission, and the capacity of self-floating, the PFC foam can be an attractive material for efficient solar steam generation and wastewater purification. Moreover, the material exhibits excellent stability over multiple cycles indicating its reusability in practical applications. Utilization of low cost materials such as cotton and low plasmonic metal loading leads to fabricate an economically feasible material compared to other desalination techniques such as reverse osmosis and membrane-based filters.

Supporting Information

Supporting information includes **Figure S1** showing the experimental set up used for the solar steam generation experiments, **Figure S2** displaying digital images of the steam generation by the PFC samples under optical concentration of C_{opt} = 8, **Figure S3** showing the solar evaporation data of three samples using a solar light density of 5 kW m^{-2}, and **Figure S4** showing the temperature profile at the irradiation surface of different PFC samples under solar light density of 1 kW m^{-2}. A video for the steam generation is also provided.

## Acknowledgements

Corresponding Author

M. Samy El-Shall: Fax: 804-828-8599. Tel: 804-387-1728. E-mail: mselshal@vcu.edu.

References

1. Siva Reddy, V.; Kaushik, S.; Ranjan, K.; Tyagi, S. State-of-the-Art of Solar Thermal Power Plants. A Review. *Renewable Sustainable Energy Rev*. **2013**, 27, 258–273.
2. Sharon, H.; Reddy, K. S. A review of solar energy driven desalination technologies. *Renewable Sustainable Energy Rev.* **2015**, 41, 1080–1118.
3. Chandrashekara, M.; Yadav, A. Water Desalination System Using Solar Heat: A Review. *Renewable Sustainable Energy Rev*. **2017**, 67, 1308–1330.
4. Zhang, L. B.; Tang, B.; Wu, J. B.; Li, R. Y.; Wang, P. Hydrophobic Light-to-Heat Conversion Membranes with Self-Healing Ability for Interfacial Solar Heating. *Adv. Mater*. **2015**, 27, 4889–4894.
5. Surwade, S. P.; Smirnov, S. N.; Vlassiouk, I. V.; Unocic, R. R.; Veith, G. M.; Dai, S.; Mahurin, S. M., Water desalination using nanoporous single-layer graphene. *Nature Nanotech.* **2015**, 10, 459–464.
6. Ni, G.; Li, G.; Boriskina, S. V.; Li, H. X.; Yang, W. L.; Zhang, T. J.; Chen, G. Steam Generation under One Sun Enabled by a Floating Structure with Thermal Concentration. *Nat. Energy* **2016**, 1, 16126–16132.
7. Politano, A.; Argurio, P.; Di Profio, G.; Sanna, V.; Cupolillo, A.; Chakraborty, S.; Arafat, H. A.; Curcio, E. Photothermal Membrane Distillation for Seawater Desalination. *Adv. Mater*. **2017**, 29, 1603504.
8. Xu. N.; Hu, X.; Xu, W.; Li, X.; Zhou, L.; Zhu, S.; Zhu, J. Mushrooms as Efficient Solar Steam-Generation Devices. *Adv. Mater*. **2017**, 29, 1606762.
9. Aubry, A.; Lei, D. Y.; Fernández-Domínguez, A. I.; Sonnefraud, Y.; Maier, S. A.; Pendry, J. B., Plasmonic

Light-Harvesting Devices over the Whole Visible Spectrum. *Nano Lett.* **2010**, 10, 2574-2579.

10. Hogan, N. J.; Urban, A. S.; Ayala-Orozco, C.; Pimpinelli, A.; Nordlander, P.; Halas, N. J. Nanoparticles Heat through Light Localization. *Nano Lett*. **2014**, 14, 4640-4645.

11. Bae, K.; Kang, G. M.; Cho, S. K.; Park, W.; Kim, K.; Padilla, W. J. Flexible Thin-Film Black Gold Membranes with Ultrabroadband Plasmonic Nanofocusing for Efficient Solar Vapour Generation. *Nat. Commun*. **2015**, 6, 10103–10111.

12. Zhou, L.; Tan, Y. L.; Wang, J. Y.; Xu, W. C.; Yuan, Y.; Cai, W. S.; Zhu, S. N.; Zhu, J. 3D Self-Assembly of Aluminium Nanoparticles for Plasmon-Enhanced Solar Desalination. *Nat. Photonics* **2016**, 10, 393–398.

13. Zhou, L.; Zhuang, S. D.; He, C. Y.; Tan, Y. L.; Wang, Z. L.; Zhu, J. Self-Assembled Spectrum Selective Plasmonic Absorbers with Tunable Bandwidth for Solar Energy Conversion. *Nano Energy* **2017**, 32, 195–200.

14. Zhou, L.; Zhuang, S. D.; He, C. Y.; Tan, Y. L.; Wang, Z. L.; Zhu, J. Self-Assembled Spectrum Selective Plasmonic Absorbers with Tunable Bandwidth for Solar Energy Conversion. *Nano Energy* **2017**, 32, 195–200.

15. Govorov, A. O.; Richardson, H. H. Generating Heat with Metal Nanoparticles. *Nano Today* **2007**, 2, 30–38.

16. Oara Neumann, Alexander S. Urban, Jared Day, Surbhi Lal, Peter Nordlander, and Naomi J. Halas**,** Solar Vapor Generation Enabled by Nanoparticles, *ACS Nano* **2013**, 7, 42-49.

17. Ghasemi, H.; Ni, G.; Marconnet, A. M.; Loomis, J.; Yerci, S.; Miljkovic, N.; Chen, G., Solar steam generation by heat localization. *Nature Commun.* **2014**, 5, 5449.

18. Zhu, M.; Li, Y.; Chen, F.; Zhu, X.; Dai, J.; Li, Y.; Yang, Z.; Yan, X.; Song, J.; Wang, Y., Plasmonic Wood for High-Efficiency Solar Steam Generation. *Adv. Energy Mater.* **2017**, 1701028.

19. Li, X. Q.; Xu, W. C.; Tang, M. Y.; Zhou, L.; Zhu, B.; Zhu, S. N.; Zhu, J. Graphene Oxide-Based Efficient and Scalable Solar Desalination under One Sun with a Confined 2D Water Path. *Proc. Natl. Acad. Sci. U. S. A.* **2016**, 113, 13953–13958.

20. Hu, X.; Xu, W.; Zhou, L.; Tan, Y.; Wang, Y.; Zhu, S.; Zhu, J. Tailoring Graphene Oxide-Based Aerogels for Efficient Solar Steam Generation under One Sun. *Adv. Mater*. **2017**, 29, 1604031.

21. Wang, G.; Fu, Y.; Guo, A.; Mei, T.; Wang, J.; Li, J.; Wang, X., Reduced graphene oxide-polyurethane nanocomposite foams as a reusable photo-receiver for efficient solar steam generation. *Chem. Mater.* **2017**, 29, 5629-5635.

22. Zhang, P.; Li, J.; Lv, L.; Zhao, Y.; Qu, L., Vertically Aligned Graphene Sheets Membrane for Highly Efficient Solar Thermal Generation of Clean Water. *ACS Nano* **2017**, 11, 5087-5093.

23. Yang, J.; Pang, Y.; Huang, W.; Shaw, S. K.; Schiffbauer, J.; Pillers, M. A.; Mu, X.; Luo, S.; Zhang, T.; Huang, Y., Functionalized Graphene Enables Highly Efficient Solar Thermal Steam Generation. *ACS Nano* **2017,** 11, 5510-5518.

24. Awad, F. S.; Kiriarachchi, H. D.; AbouZeid, K. M.; Özgür, Ü.; El-Shall, M. S., Plasmonic Graphene Polyurethane Nanocomposites for Efficient Solar Water Desalination. *ACS Applied Energy Materials* **2018,** 1, 976-985.

25. Pongprayoon, T.; O'Rear, E. A.; Yanumet, N.; Yuan, W. L. Wettability of Cotton Modified by Admicellar Polymerization. *Langmuir* **2003**, 19, 3770-3778.

26. Chen, S.; Li, X.; Li, Y; Sun, J. Intumescent Flame-Retardant and Self-Healing Superhydrophobic Coatings on Cotton Fabric. *ACS Nano* **2015**, 9, 4070-4076.

27. Hassan, H. M.; Abdelsayed, V.; Abd El Rahman, S. K.; AbouZeid, K. M.; Terner, J.; El-Shall, M. S.; Al-Resayes, S. I.; El-Azhary, A. A., Microwave synthesis of graphene sheets supporting metal nanocrystals in aqueous and organic media. *J. Mater. Chem.* **2009,** 19, 3832-3837.

28. Siqueira, G.; Bras, J.; Dufresne, A., New process of chemical grafting of cellulose nanoparticles with a long chain isocyanate. *Langmuir* **2009,** *26* (1), 402-411.

29. Tursi, A.; Beneduci, A.; Chidichimo, F.; De Vietro, N.; Chidichimo, G., Remediation of hydrocarbons polluted water by hydrophobic functionalized cellulose. *Chemosphere* **2018,** *201*, 530-539.

30. Zedan, A. F.; Moussa, S.; Terner, J.; Atkinson, G.; El-Shall, M. S., Ultrasmall Gold Nanoparticles Anchored to Graphene and Enhanced Photothermal Effects by Laser Irradiation of Gold Nanostructures in Graphene Oxide Solutions. *ACS Nano* **2013,** *7* (1), 627-636.

31. Moussa, S.; Atkinson, G.; El-Shall, M. S.; Shehata, A.; AbouZeid, K. M.; Mohamed, M. B. Laser Assisted Photocatalytic Reduction of Metal Ions by Graphene Oxide. *J. Mater. Chem.* **2011**, 21, 9608-19.

32. https://www.nrel.gov/grid/solar-resource/spectra-am1.5.html (accessed Aug 27, 2018).

33. Matolín, V.; Cabala, M.; Matolínová, I.; Škoda, M.; Libra, J.; Václavů, M.; Prince, K. C.; Skála, T.; Yoshikawa, H.; Yamashita, Y.; Ueda, S.; Kobayashi, K., Au^+ and Au^{3+} ions in CeO_2 rf-sputtered thin films. *Journal of Physics D: Applied Physics* **2009,** *42* (11), 115301.

34. Matsumoto, T.; Nickut, P.; Tsunoyama, H.; Watanabe, K.; Tsukuda, T.; Al-Shamery, K.; Matsumoto, Y., Thermal and photochemical

reactivity of oxygen atoms on gold nanocluster surfaces. *Surface Science* **2007,** *601* (22), 5226-5231.

35. Deng, Q.; Duan, X.; Ng, D. H. L.; Tang, H.; Yang, Y.; Kong, M.; Wu, Z.; Cai, W.; Wang, G., Ag Nanoparticle Decorated Nanoporous ZnO Microrods and Their Enhanced Photocatalytic Activities. *ACS Applied Materials & Interfaces* **2012,** *4* (11), 6030-6037.

36. Schmidt, M.; Masson, A.; Bréchignac, C., Oxygen and Silver Clusters: Transition from Chemisorption to Oxidation. *Physical Review Letters* **2003,** *91* (24), 243401.

37. Agnihotri, S.; Bajaj, G.; Mukherji, S.; Mukherji, S., Arginine-assisted immobilization of silver nanoparticles on ZnO nanorods: an enhanced and reusable antibacterial substrate without human cell cytotoxicity. *Nanoscale* **2015,** *7* (16), 7415-7429.

38. Abbas, A.; Zhao, Y.; Zhou, J.; Wang, X.; Lin, T., Improving thermal conductivity of cotton fabrics using composite coatings containing graphene, multiwall carbon nanotube or boron nitride fine particles. *Fibers and Polymers* **2013,** *14* (10), 1641-1649.

39. Jiang, Q.; Tian, L.; Liu, K. K.; Tadepalli, S.; Raliya, R.; Biswas, P.; Naik, R. R.; Singamaneni, S., Bilayered biofoam for highly efficient solar steam generation. *Adv. Mater*. **2016**, 28, 9400-9407.

40. Xue, G.; Liu, K.; Chen, Q.; Yang, P.; Li, J.; Ding, T.; Duan, J.; Qi, B.; Zhou, J., Robust and Low-Cost Flame-Treated Wood for High-Performance Solar Steam Generation. *ACS Appl. Mater. Interfaces* **2017**, 9, 15052-15057.

41. Adham, S.; Hussain, A.; Matar, J. M.; Dores, R.; Janson, A., Application of Membrane Distillation for desalting brines from thermal desalination plants. *Desalination* **2013,** *314*, 101-108.

42. Hammer, B.; Norskov, J. K., Why gold is the noblest of all the metals. *Nature* **1995,** *376*, 238.

43. Badawy, A. M. E.; Luxton, T. P.; Silva, R. G.; Scheckel, K. G.; Suidan, M. T.; Tolaymat, T. M., Impact of Environmental Conditions (pH, Ionic Strength, and Electrolyte Type) on the Surface Charge and Aggregation of Silver Nanoparticles Suspensions. *Environmental Science & Technology* **2010,** *44* (4), 1260-1266.
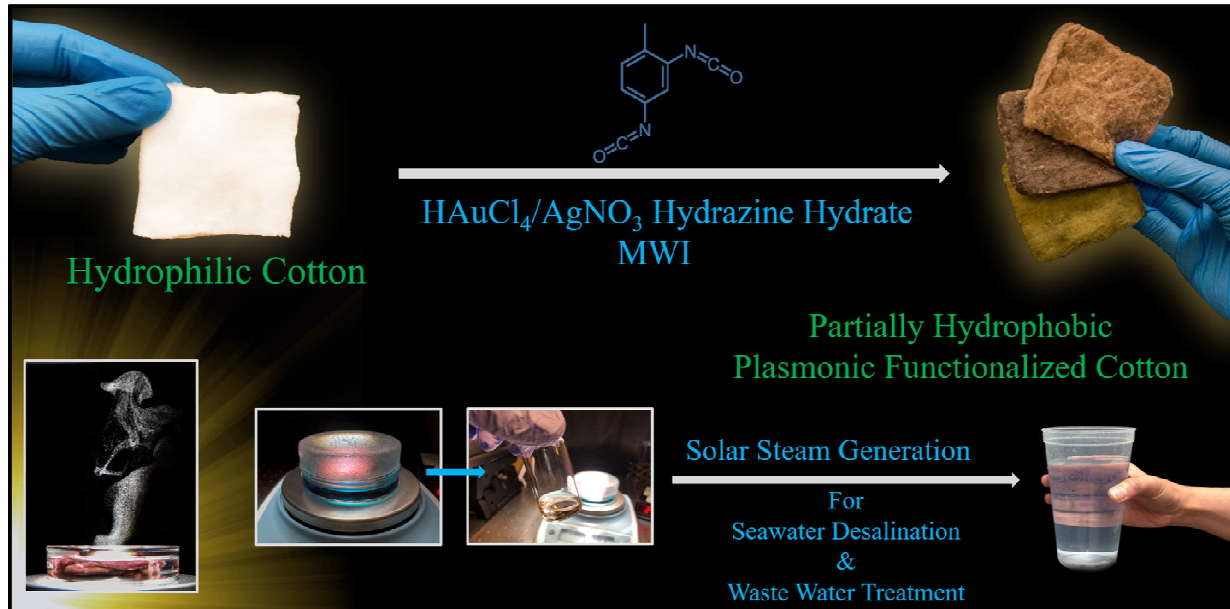
Highly efficient, flexible, low weight, and cost effective *Plasmonic Functionalized Cotton (PFC)* nanocomposites for efficient solar desalination and wastewater purification.